


Elimination of Severe Near-Field Spatial Variations of Ultrasonic Transducers Using γ -Power Bessel Function Amplitude Distribution

Qi Zhou,¹ Rui Zhang,¹ and Wenwu Cao^{1,2,*}

¹*Condensed Matter Science and Technology Institute, School of Instrumentation Science and Engineering, Harbin Institute of Technology, Harbin 150080, China*

²*Department of Mathematics and Materials Research Institute, The Pennsylvania State University, University Park, Pennsylvania 16802, USA*

 (Received 24 July 2019; revised manuscript received 5 September 2019; published 27 September 2019)

Many published biomedical and chemical experimental results involving ultrasound suffer inconsistencies. One of the main reasons is due to the nonuniform field produced by conventional piston-type ultrasonic transducers; severe intensity fluctuation occurs in the near-field region where most experiments are conducted. We show both theoretically and experimentally that if the transducer surface vibration can be controlled to have an amplitude distribution in the form of $J_0[(\rho/R_0)^\gamma U_1]$, where ρ is the radial coordinate, R_0 is the radius of the acoustic source, $\gamma \geq 1$, and U_1 is the first zero of the zeroth-order Bessel function of the first kind $J_0(r)$, then the pressure amplitude space variation in the near-field can be eliminated to produce a three-dimensional (3D) cylindrical region with uniform pressure distribution near the transducer surface. The width of the cylindrical region increases while its height decreases with γ , which gives the flexibility of manipulating the shape of the uniform pressure field region. The presented design is beneficial for many biomedical and chemical experiments, as well as industrial applications that require uniform pressure sonication.

DOI: [10.1103/PhysRevApplied.12.034056](https://doi.org/10.1103/PhysRevApplied.12.034056)

I. INTRODUCTION

Diffraction is a ubiquitous manifestation of coherent waves, including mechanical (acoustic) waves, electromagnetic waves, and de Broglie waves in quantum mechanics. For a circular coherent wave source with finite aperture, the transverse beam profile in the far field is featured with an Airy disk and its transverse dimension expands with propagation distance. As a nondiffracting solution of the free space wave equation, Bessel-type beams have been introduced to neutralize this divergent effect, which could maintain its transverse beam profile to be independent of propagation distance. Bessel beams have been applied in a wide range of applications, including, but not limited to, transmission electron microscopy, optical microscopy [1,2], micromanipulation of small particles [3], three-dimensional (3D) fluorescence imaging [4], diagnostic ultrasound [5–7], etc. Such nondiffracting beam studies mainly concern the counterbalancing of transverse spreading of waves after long-distance propagation. However, in other applications, such as holography, interferometry, and ultrasonic therapy, the requirement for wave beams is different. A uniform transverse profile across a finite distance is demanded and the transverse dimension also needs to have a certain size.

Conventional Bessel beams with a prominent narrow central peak do not meet this requirement. Typical solutions for optical applications are beam-shaping techniques that convert a Gaussian irradiance profile to a flat-topped one. However, because of diffraction, the stable working depth of the converted beam is quite limited since its uniform profile cannot be preserved across a long distance.

In most ultrasonic applications, such as ultrasound-mediated gene transfer [8], membrane sonoporation [9,10], sonodynamic therapy [11–15], and ultrasound cleaning [16], piston sources are most commonly employed. Ultrasound plays its role via the interaction with tiny gas bubbles in the fluid, i.e., via acoustic cavitation [17,18]. The dynamic characteristics of acoustically driven bubbles are sensitive to the amplitude of ultrasound. Different degrees of cavitation could exert diverse types of impacts on the surroundings, e.g., inertial and noninertial cavitation effects, depending on the ultrasound intensity [19]. As a result, such ultrasonic investigations inevitably suffer from the beam-intensity nonuniformity of ultrasound.

Specifically, consider ultrasound propagation from a circular piston transducer of radius R_0 to the half-space ($z > 0$); its typical characteristic distance z_0 (Rayleigh distance) is given by $z_0 \approx R_0^2 f/v$, where f is the frequency and v is the sound velocity in the medium. The near-field region refers to the region from the transducer surface to

*dzk@psu.edu

z_0 , in which the pressure amplitude of ultrasound fluctuates drastically. The acoustic pressure amplitude changes from point to point in space and there are many intensity minima and maxima inside the near-field region, a large number of points in this region even have nearly zero field intensity (hollow pores).

Taking *in vitro* biomedical ultrasound experiments in cancer research as an example, cells are attached to the bottom of the incubation dish of a certain size, and the dish is placed in the near-field region of an ultrasonic transducer. Cells distributed in the near-field region cannot be exposed equally due to the intrinsic nature of the nonuniform near field. Besides, sonication in the far-field region suffers the same problem as Bessel beams: the intensity profile in the far field is sharply peaked. On the other hand, because of dimensional constraints, most biomedical, chemical, and industrial applications of ultrasound use the near field because the far field is too far away for larger size transducers. The severe variation of ultrasonic intensity in the near field has caused a great deal of inconsistent data in the literature, producing some misleading results [20,21]. To fulfill the requirement of large-area uniform irritation across a finite distance, we present here a method to achieve a large-scale 3D cylindrical region near the transducer surface where the wave amplitude is practically uniform.

II. THEORY

A. Nondiffraction beam

As a nondiffracting solution of the scalar wave equation, an axial symmetric Bessel beam that propagates along the z axis can be described by

$$\varphi(\mathbf{r}, t) = J_0(\alpha\rho)e^{i(\beta z - \omega t)}, \quad (1)$$

where φ represents the wave potential, J_0 is the zeroth-order Bessel function of the first kind, $\mathbf{r} = (x, y, z)$ represents the vector coordinates of the observing point in space, $\rho = (x^2 + y^2)^{1/2}$ is the distance away from the center axis of the source, α is a scaling parameter with $\beta^2 + \alpha^2 = k^2$, and k represents the wave number.

In the current study, we focus on the uniform irritation issue of ultrasound beams. Assuming a Bessel acoustic source is composed of a center disk and an infinite number of contiguous annuluses with the inner radius U_n and outer radius U_{n+1} , where $U_n(\alpha)$ denotes the n th zeros of $J_0(\alpha\rho)$. According to the superposition principle, the pressure on the central axis (z axis) can be written as [22]

$$P_n(r) = \frac{A_0 k}{2\pi} \int_{U_n}^{U_{n+1}} J_0(\alpha\rho) \frac{e^{ikr}}{r} \rho d\rho, \quad (2)$$

where A_0 denotes the pressure amplitude at the origin point. The center disk is described by $n = 0$ and $U_0 = 0$ in Eq. (2).

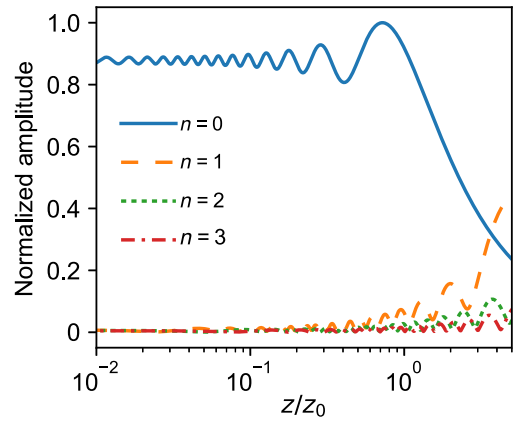


FIG. 1. Normalized amplitude distribution of the first four elements ($n = 0-3$) along the central axis calculated using Eq. (2).

Figure 1 illustrates the normalized amplitude distribution of the first four elements ($n = 0-3$, $\alpha = 96.2$, $U_1 = R_0 = 25$ mm, $z_0 = 416$ mm, $v = 1500$ m/s, $f = 1$ MHz, and $kR_0 = 104.7$) along the central axis, which was calculated using Eq. (2). When only the central disk is activated, the amplitude of pressure fluctuation on the central axis does not exceed 10% as long as the distance ratio $z/z_0 < 0.6$. Moreover, the results presented in Fig. 1 demonstrate that the contributions of peripheral annuluses increase with the axial distance. Most of the acoustic energy on the central axis is emitted from the center element in the near-field region; while contributions of surrounding elements become apparent only in the far-field region of $z > z_0$.

In the present study, we define that a deviation of amplitude less than 10% could be considered “uniform.” Therefore, the axial pressure of a J_0 Bessel beam truncated on the region $[0, U_1]$ can be considered uniform in the region very close to the center region of the source surface. We calculate its amplitude distribution of the ultrasound beam emitted by an acoustic source with the amplitude distribution in the form of J_0 truncated to the central element only, i.e., in $[0, U_1]$. Figures 2(a) and 2(b) show the near field of a 25-mm radius piston transducer; one can see that a large number of maximum and minimum nodes exist. On the other hand, the distribution of the ultrasound energy emitted by a 25-mm-radius ($\alpha = 96.2$) center disk of a Bessel distribution transducer shows a very different feature as shown in Fig. 2(c). Its lateral pressure variation at $z/z_0 = 0.05, 0.1, 0.25$, and 0.5 , respectively, are extracted and presented in Fig. 2(d). As revealed in Fig. 1, the pressure amplitude along the axis is uniform in the region of $z/z_0 < 0.25$. It is rather encouraging, but the downside of this design is that its lateral distribution of ultrasound amplitude is not uniform; the pressure amplitude decreases rapidly along the radial direction as shown in Fig. 2(d).

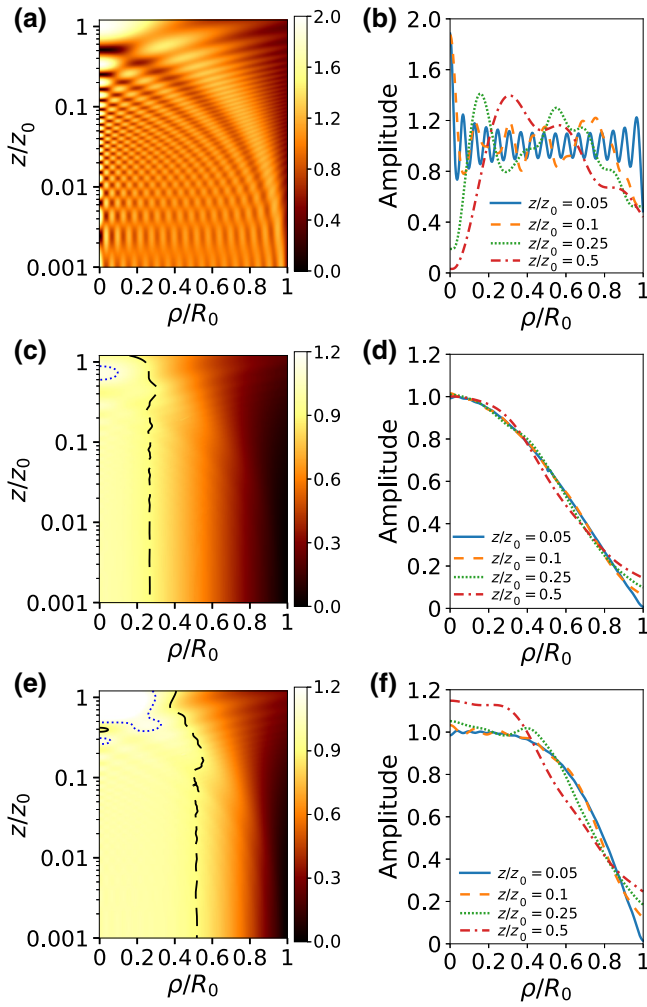


FIG. 2. Spatial distribution of pressure amplitude in the axial plane generated by a 1 MHz circular acoustic source. (a) Piston-type uniform amplitude distribution, (c) J_0 -type acoustic source truncated on $[0, U_1]$, (e) B_2 -type amplitude distribution; the lateral profiles at $z/z_0 = 0.05, 0.1, 0.25,$ and 0.5 are presented in (b),(d),(f), respectively. All three types of sources have the same radius of 25 mm. The dashed lines in (c),(e) represent contour amplitude levels of $\pm 10\%$. The pressure amplitude has been normalized by the source amplitude at $\rho = 0$.

B. Creating a wider uniform region using γ -power zeroth-order Bessel function amplitude distribution

For many practical applications, a sizable 3D region of uniform ultrasonic exposure is needed. For example, in biomedical experiments, the cell dish has a certain size and the whole cell dish must have the same level of ultrasound exposure to guarantee that the results are meaningful. We have tried many different types of amplitude space distributions aiming to widen the Bessel beam, and finally we find that a γ -power zeroth-order Bessel function of the first kind (B_γ) truncated within the region bounded by the first zero $[0, R_0]$ can serve this purpose. Specifically,

the function is given by

$$B_\gamma(\rho) = J_0\left(\left[\frac{\rho}{R_0}\right]^\gamma U_1\right), \quad (3)$$

where R_0 denotes the radius of the circular radiating source, U_1 (approximately 2.4048) denotes the first zero of $J_0(r)$, and $\gamma \geq 1$. Apparently, B_γ becomes flatter as γ increases and goes to a constant on $[0, R_0)$ when $\gamma \rightarrow \infty$, which corresponds to the traditional piston transducer. The pressure distribution of a B_γ acoustic source with a radius of R_0 can be calculated by [22]

$$P(r) = \frac{A_0 k}{2\pi} \int_0^{2\pi} \int_0^{R_0} J_0\left(\left[\frac{\rho}{R_0}\right]^\gamma U_1\right) \frac{e^{ikR}}{2\pi R} \rho d\rho d\theta, \quad (4)$$

where $R = |r - r'(\rho, \theta)|$ denotes the distance between the observation point and the point on the source surface. When $\gamma = 2$, the acoustic field on the axial plane in the near-field region is shown in Figs. 2(e) and 2(f). The dashed line and dotted line represent the contour amplitude levels of 90% and 110%, respectively, forming a uniform region nearly two times as wide as that of the case of $\gamma = 1$ [Fig. 2(c)]. The lateral profiles of the beam in this region are much flatter than that of the J_0 beam.

The beam shape along the central axis is well maintained in the whole region from 0 to $0.5z_0$ when $\gamma = 1$ [Fig. 2(d)]. The pressure amplitude along the z axis fluctuates more with the increase of γ , accompanied by the increase of the radius of this cylindrical uniform region. As shown in Fig. 2(f), the upper limit of the uniform region along the axial direction decreases to $0.28z_0$ when $\gamma = 2$. When $\gamma = 3$ and $\gamma = 4$, the height of this uniform cylindrical region decreases to $0.17z_0$ and $0.11z_0$, respectively, while the corresponding width of this uniform region increases to $0.65R_0$ and $0.71R_0$, respectively. For the 25-mm-radius example case with $\gamma = 4$, the height of this cylindrical region is $0.11z_0 = 45.8$ mm, while the radius becomes 17.75 mm; the uniform 3D region is still quite large. A wider but shorter cylindrical region is more suitable for biomedical experiments using a cell dish since the dish height is rather short. Calculated results for cases of γ from 1 to 5 are listed in Table I. Specifically, for a 1-MHz ultrasound to uniformly sonicate on a cell dish with a radius of 17.5 mm, we can make a B_γ source with a transducer radius of $R_0 = 33$ mm. The corresponding height of the uniform cylindrical region along the z axis is 229 mm, which well satisfies most experimental requirements.

It is worth noting that the scalar diffraction theory is appropriate when the wavelength is much smaller compared to R_0 [23]. Obviously, this criterion cannot be satisfied at a very small R_0 or very low frequencies. Larger uniform regions could be obtained using this B_γ amplitude distribution design only with a larger R_0 or higher frequencies.

TABLE I. Calculated height and radius of the uniform cylindrical region for γ from 1 to 5 for a 25 mm-radius B_γ acoustic source at the frequency of 1 MHz.

	$\gamma = 1.0$	$\gamma = 2.0$	$\gamma = 3.0$	$\gamma = 4.0$	$\gamma = 5.0$
Height of uniform region	$0.60z_0$	$0.28z_0$	$0.17z_0$	$0.11z_0$	$0.09z_0$
Radius of uniform region	$0.26R_0$	$0.52R_0$	$0.65R_0$	$0.71R_0$	$0.76R_0$

The above results demonstrate that this innovative B_γ -type source design could eliminate the severe near-field variations to create a sizable 3D cylindrical region with uniform ultrasound amplitude, making it possible for experimental objects, such as cells in an incubation dish or chemicals in a beaker to expose a similar level of ultrasound to guarantee the consistency of experimental results.

III. STEPPED DESIGN FOR PRACTICAL IMPLEMENTATION

When an annular array transducer is employed for beamforming, smoothly and continuously varying the amplitude on the radiating surface of a transducer requires an infinite number of elements, which is impractical. Instead, stepped amplitude modulation with a finite number of elements can be easily realized. We investigate the performance degradation induced by this compromise. For the case of $\gamma = 2$, we assume that the outer radius of the 1-MHz annular transducer is 25 mm, containing a certain number of equal-area annular elements (for example, $N = 10$ and 15). The output amplitude changes from element to element according to the γ -power Bessel function. The step function amplitude distribution is shown in Fig. 3(a) and the corresponding beam profiles for $N = 10$ and 15 are shown in Figs. 3(b) and 3(d), respectively. To intuitively see the useful region in both cases, a smaller region ($0-0.5z_0$, $0-0.6R_0$) was enlarged and redrawn in Figs. 3(c) and 3(e). We can see that $N = 10$ is not enough because the near-field amplitude shows strong variations in the region of $z < 0.05z_0$, while $N = 15$ is sufficient to eliminate most of the variations in the very near field. Of course, larger N will be better for approaching the continuous function to completely eliminate the drastic amplitude variation in the near-field, but it will increase the difficulty in the annular array transducer fabrication. Based on our calculations, there is practically no difference between the continuous and step function distributions when $N = 20$.

As an example, we calculated a 1-MHz circular source of 25-mm radius to quantitatively show the effective 3D region of uniform amplitude. When we use 15 annular elements of equal area, the uniform cylindrical region near the acoustic source will be 100 mm in height with a radius of about 13 mm. The near-field variation is practically smoothed out inside this region.

In general, using the design principle given here, one could easily create a desired 3D near-field region with

uniform pressure amplitude by controlling the radius of the transducer and the value of γ . In addition, as shown in Fig. 3(a), for an equal radiating surface, the width of the

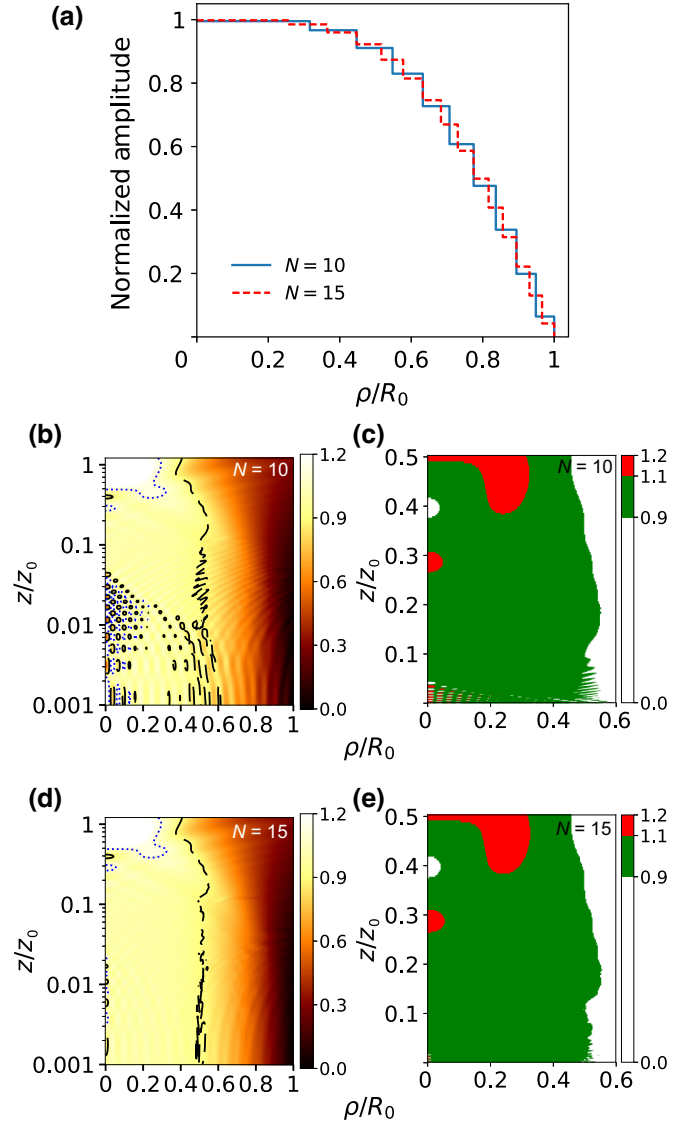


FIG. 3. (a) Stepped-amplitude modulation of two partition numbers (dashed line, $N = 10$; dotted line, $N = 15$). Spatial distribution of pressure amplitude in the axial plane at a partition number of 10 (b) and 15 (d). Their linear coordinates forming a smaller space ($0-0.5z_0$, $0-0.6R_0$) were redrawn in (c) $N = 10$, and (e) $N = 15$; green maps indicate the uniform region. The pressure amplitude has been divided by the source amplitude at $\rho = 0$.

annular element decreases monotonically from the center to the edge. For example, in the presented case above, the geometric aspect ratio in the center element is approximate 0.1, while the outmost one is more than 1. Their electromechanical coupling factor changes from k_t (plate mode) toward k_{33} (bar mode) [24]. This change of electromechanical coupling factor from element to element causes great difficulties in practical control of the surface vibration amplitude, and there is a transverse mode coupling for the k_t mode, making things even worse. To overcome this problem, we employ 1–3-type piezoelectric composite to make the transducer [25], which makes all elements vibrate in the k_{33} mode when the lateral dimension of the ceramic rods is sufficiently small. We also found that using 1–3 composite could further reduce the number of elements needed to effectively approximate the continuous B_γ amplitude distribution, owing to the coupling between ceramic rods.

IV. EXPERIMENTAL VALIDATION

The new transducer design can be realized using annular elements without phase modulation, so that only one channel electronic source is needed. The manipulation of surface vibration amplitude can be achieved by connecting different resistors to those parallel-connected annular elements.

To overcome the issue of the aspect-ratio-dependent electromechanical coupling factor, we employ 1–3-type piezoelectric composite elements to produce the B_γ beams. A 25-mm-diameter 1–3 composite plate was made of lead

zirconate titanate ceramic (PZT-4) rods and epoxy resin. The thickness of the 1–3 composite plate at 1 MHz is 1.574 mm, while its pitch (PZT rods) and kerf (epoxy filler) widths are 0.3 and 0.15 mm, respectively. We utilize laser ablation to cut one side of the electrode on the plate surface into ten equal-area concentric rings based on our simulation results. A structural illustration of the composite plate is shown in Fig. 4(a), and the insert is a magnified portion of the real composite plate. The applied voltage on each subelectrode is modulated by the resistor connected to each element in series. All annular elements are connected to the same power source in parallel.

The profiles of the produced B_2 and B_3 beams are measured in degassed water using a needle hydrophone that is attached to a 3D precise positioning system. In addition, the finite-element software COMSOL is employed to simulate the pressure field and electrical impedance curves. As shown in Fig. 4(b), both simulated and measured composite plates resonate at 1 MHz; the slight disparity is caused by the missing mechanical loss in the simulation.

The simulated surface vibration amplitude distribution of the transducer is shown in Fig. 4(c). In the central region of the plate, the vibration amplitude is about 85 nm/V. The distribution of the vibration amplitude well matches the shape of B_2 and B_3 functions with the same radius [the dark dotted lines in Fig. 4(c)]. The fluctuating feature of the amplitude distribution originates from the acoustic impedance mismatch between the ceramic and epoxy phase. On the other hand, this acoustic mismatch helps localize the vibration energy of each element and inhibits

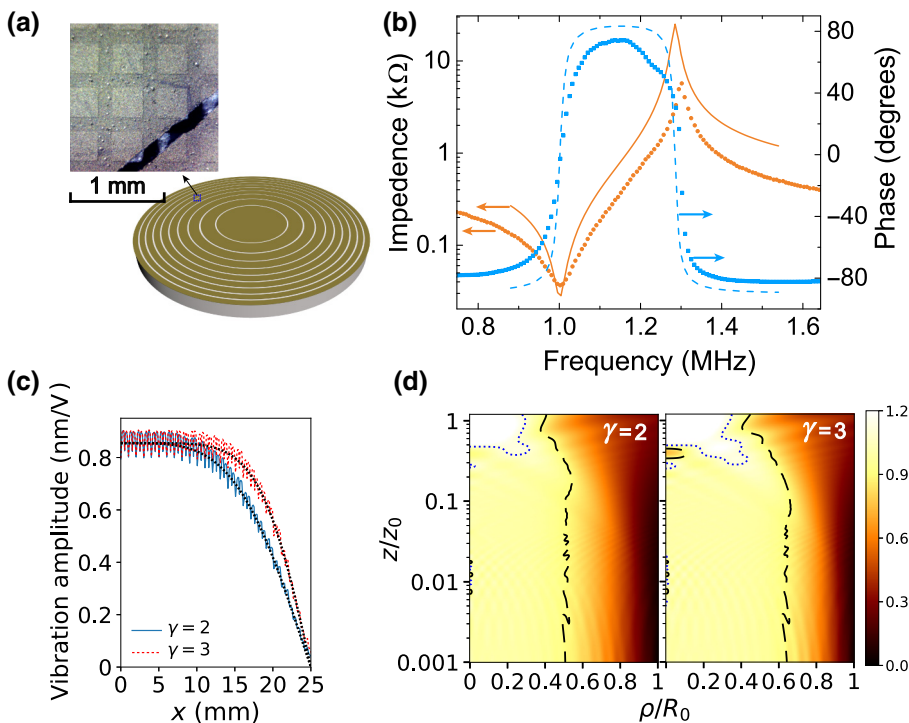


FIG. 4. (a) Illustration of 1–3 composite plate annular array transducer design (not in real scale) which was used to generate B_2 and B_3 beams (the insert is optical microscope image of the real composite). (b) Simulated (solid line, amplitude; dashed line, phase) and measured (circle, amplitude; square, phase) electrical impedance of the composite plate. (c) Simulated vibration amplitude on the plate surface. (d) Simulated near-field pressure distributions of B_2 and B_3 beams.

the interference of the transverse mode so that the field becomes quite uniform when the element number $N = 10$.

The simulated near-field pressure distributions of B_2 and B_3 transducers presented in Fig. 4(d) are in agreement with the integration results shown in Fig. 2. Different from the results shown in Fig. (3), no severe variations are observed in the region of $z < 0.05z_0$, although the driving signal applied on the composite plate only consists of 10 stepped amplitudes ($N = 10$). This shows the advantage of using 1–3 composite material to make the B_γ transducer. The cross talk between nearby pitches smoothes the vibration energy over the plate, which eliminates the stepped change of amplitude distribution. As a result, $N = 10$ was adequate for this validation experiment when the 1–3 composite was employed.

As shown in Figs. 5(a) and 5(b), for B_2 and B_3 beams, the measured pressure produced by our transducer along the beam axis is almost constant in the region of $0 < z < 80$ mm. The measured B_2 beam has a uniform length of $0.277z_0$ (115 mm), while the measured B_3 beam has a uniform length of $0.264z_0$ (110 mm). Both of them

are in agreement with the simulated data represented in Figs. 4(d) and 4(e). The lateral features of B_2 and B_3 beams (at $z/z_0 = 0.05, 0.1, 0.25,$ and 0.5) are shown in Fig. 5(c). The measured beam shapes are also consistent with simulated data in the near-field region.

V. SUMMARY AND CONCLUSIONS

In conclusion, we present an innovative design for an ultrasonic transducer with a surface vibration amplitude distribution that follows the γ -power zeroth-order Bessel function given by Eq. (3), which can smooth out the severe spatial variation of the near field to produce a cylindrical 3D region with uniform amplitude. When the transducer aperture is fixed, the radius of this uniform region can be enlarged by increasing the exponent γ in Eq. (3) at the expense of shortening the height of the uniform region along the axial direction. It is important for the transducer aperture to satisfy the relationship of $kR_0 > 30$ in order for the design to work. In other words, a lower frequency needs a larger-radius transducer. We also provide a practical way to realize this design using annular array elements made of 1–3 piezoelectric composite material with only a one-channel electric driving power source. The amplitude of each element can be controlled by connecting different resistors to each element under the same applied electric voltage. The B_2 and B_3 transducers that we make utilizing 1–3-type piezoelectric composite plates validate our design. The simulated results and measured data for the 1–3 composite transducers are in very good agreement, providing a solid support for the idea.

The current invention can help resolve the inconsistency issue that has been troubling researchers in many biomedical and chemical experiments that require a relatively uniform sonication region with a sizable volume. The idea may also be used in other fields involving coherent wave propagation, such as optical holography, holographic transmission electron microscopy, optical interferometry, etc., in which a sizable 3D uniform irradiation region is needed.

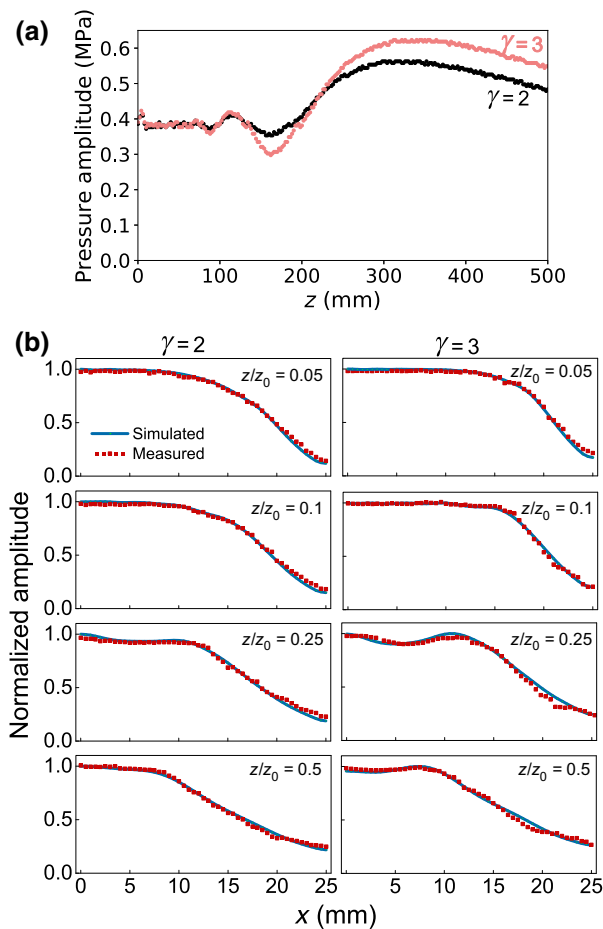


FIG. 5. Near-field feature of B_2 and B_3 beams measured by a needle hydrophone. (a) Amplitude distribution along the central axis. (b) Lateral amplitude distribution at $z/z_0 = 0.05, 0.1, 0.25$ and 0.5 .

[1] F. O. Fahrbach, P. Simon, and A. Rohrbach, Microscopy with self-reconstructing beams, *Nat. Photonics* **4**, 780 (2010).
 [2] V. Grillo, E. Karimi, G. C. Gazzadi, S. Frabboni, M. R. Dennis, and R. W. Boyd, Generation of Nondiffracting Electron Bessel Beams, *Phys. Rev. X* **4**, 1 (2014).
 [3] V. Garcés-Chávez, D. McGloin, H. Melville, W. Sibbett, and K. Dholakia, Simultaneous micromanipulation in multiple planes using a self-reconstructing light beam, *Nature* **419**, 145 (2002).
 [4] L. Gao, L. Shao, B.-C. Chen, and E. Betzig, 3D live fluorescence imaging of cellular dynamics using Bessel beam plane illumination microscopy, *Nat. Protoc.* **9**, 1083 (2014).

- [5] J.- Lu and J. F. Greenleaf, Ultrasonic nondiffracting transducer for medical imaging, *IEEE Trans. Ultrason. Ferroelectr. Freq. Control* **37**, 438 (1990).
- [6] J.-Y. Lu and J. F. Greenleaf, Pulse-echo imaging using a nondiffracting beam transducer, *Ultrasound Med. Biol.* **17**, 265 (1991).
- [7] D. Ding and J. H. Huang, Second-harmonic generation of limited diffraction beams, *J. Opt. A: Pure Appl. Opt.* **9**, 1131 (2007).
- [8] C. M. H. Newman and T. Bettinger, Gene therapy progress and prospects: Ultrasound for gene transfer, *Gene Ther.* **14**, 465 (2007).
- [9] K. Kooiman, M. Foppen-Harteveld, A. F. W. Van Der Steen, and N. De Jong, Sonoporation of endothelial cells by vibrating targeted microbubbles, *J. Control. Release* **154**, 35 (2011).
- [10] B. Helfield, X. Chen, S. C. Watkins, and F. S. Villanueva, Biophysical insight into mechanisms of sonoporation, *Proc. Natl. Acad. Sci. U.S.A* **113**, 9983 (2016).
- [11] N. Yumita, R. Nishigaki, K. Umemura, and S. Umemura, Hematoporphyrin as a sensitizer of cell-damaging effect of ultrasound, *Jpn. J. Cancer Res.* **80**, 219 (1989).
- [12] I. Rosenthal, J. Z. Sostaric, and P. Riesz, Sonodynamic therapy—a review of the synergistic effects of drugs and ultrasound, *Ultrason. Sonochem.* **11**, 349 (2004).
- [13] P. Huang, X. Qian, Y. Chen, L. Yu, H. Lin, L. Wang, Y. Zhu, and J. Shi, Metalloporphyrin-encapsulated biodegradable nanosystems for highly efficient MRI-guided sonodynamic cancer therapy, *J. Am. Chem. Soc.* **139**, 1275 (2017).
- [14] H. Tsuru, H. Shibaguchi, M. Kuroki, Y. Yamashita, and M. Kuroki, Tumor growth inhibition by sonodynamic therapy using a novel sonosensitizer, *Free Radic. Biol. Med.* **53**, 464 (2012).
- [15] M. Trendowski, The promise of sonodynamic therapy, *Cancer Metastasis Rev.* **33**, 143 (2014).
- [16] K.-V. Jenderka and C. Koch, Investigation of spatial distribution of sound field parameters in ultrasound cleaning baths under the influence of cavitation, *Ultrasonics* **44**, e401 (2006).
- [17] P. Riesz and T. Kondo, Free radical formation induced by ultrasound and its biological implications, *Free Radic. Biol. Med.* **13**, 247 (1992).
- [18] I. Lentacker, I. De Cock, R. Deckers, S. C. De Smedt, and C. T. W. Moonen, Understanding ultrasound induced sonoporation: Definitions and underlying mechanisms, *Adv. Drug Deliv. Rev.* **72**, 49 (2014).
- [19] K. Yasui, Influence of ultrasonic frequency on multibubble sonoluminescence, *J. Acoust. Soc. Am.* **112**, 1405 (2002).
- [20] D. L. Miller, S. Bao, and J. E. Morris, Sonoporation of cultured cells in the rotating tube exposure system, *Ultrasound Med. Biol.* **25**, 143 (1999).
- [21] C. H. Fung, W. H. Cheung, N. M. Pounder, A. Harrison, and K. S. Leung, Osteocytes exposed to far field of therapeutic ultrasound promotes osteogenic cellular activities in pre-osteoblasts through soluble factors, *Ultrasonics* **54**, 1358 (2014).
- [22] K. B. Ocheltree and L. A. Frizzell, Sound field calculation for rectangular sources, *IEEE Trans. Ultrason. Ferroelectr. Freq. Control* **36**, 242 (1989).
- [23] J. Durnin, Exact solutions for nondiffracting beams. I. The scalar theory, *J. Opt. Soc. Am. A* **4**, 651 (1987).
- [24] M. Kim, J. Kim, and W. Cao, Electromechanical coupling coefficient of an ultrasonic array element, *J. Appl. Phys.* **99**, 1 (2006).
- [25] W. A. Smith and B. A. Auld, Modeling 1–3 composite piezoelectrics: thickness-mode oscillations, *IEEE Trans. Ultrason. Ferroelectr. Freq. Control* **38**, 40 (1991).